Experimental Study on Orthogonal Joints in Cross-Laminated Timber with Self-Tapping Screws installed with Mixed Angles

Justin Brown[a*], Minghao Li[a], Thomas Tannert[b], Daniel Moroder[c]

[a] Department of Civil and Natural Resources Engineering, University of Canterbury, New Zealand

[b] School of Engineering, University of Northern British Columbia Prince George, Canada

[c] PTL| Structural Consultants, Christchurch, New Zealand

Abstract

Cross-laminated timber (CLT) is increasingly being used in lateral load resisting systems of multi-storey buildings. Conventional in-plane CLT shear walls can be transformed into CLT core-wall structures with enhanced lateral strength and stiffness when the individual walls are connected orthogonally. In this paper, experimental studies are presented on orthogonal CLT joints with self-tapping screws (STS) installed with mixed angles, i.e. different installation angles between the STS axis and the plane of the CLT surface. A total of 59 orthogonal joint specimens were tested in 9 different configurations to derive the relevant joint performance parameters from monotonic and cyclic tests. The joint specimens used five-layer and seven-layer CLT panels connected by Ø8mm or Ø12mm STS. Different ratios of STS installed inclined and STS installed at 90° to the CLT surface were investigated to determine an optimum ratio of STS for enhanced joint performance. It was found that a ratio of one 90° STS for every two inclined STS ensured significant increase in ductility and displacement capacity of approximately three times when compared to specimens with only inclined STS. A minimum moderate ductility was achieved in all test series where the primary failure mode was STS withdrawal. It was found that 90° STS contributed to both strength and stiffness in joints that also contained inclined STS. The average experimental overstrength was 1.7 for most joint configurations. Existing analytical models were adequate in estimating strength but inadequate to estimate stiffness.

Keywords: Cross-laminated timber; orthogonal joints; self-tapping screws; mixed-angle installations; ductility; overstrength

* Corresponding author.
E-mail address: justin.brown@pg.canterbury.ac.nz (J. Brown)

1 Introduction

1.1 Cross-Laminated Timber Lateral Load Resisting Systems

Light timber frame (LTF) construction is very popular in North America and Oceania for low- and mid-rise residential buildings up to 6 storeys. In LTF construction, shear walls consist of vertical timber framing members to resist gravity loads and provide stability to the panel-sheathing, which is used as the lateral load resisting system (LLRS) against wind and seismic loads [1]. Post and beam timber frame construction is widely used in Japan for residential buildings up to 3 storeys in which diagonally braced or panel-sheathed shear walls are typically used as LLRS [2,3]. In the last two decades, mass timber construction has been gaining popularity due to the increased availability and cost-efficiency of engineered wood products including cross-laminated timber (CLT) and in part due to the aesthetic appeal and environmental benefits of timber as a construction material [4]. CLT is commonly composed of an odd number of layers of timber boards glued together with a crosswise layup to create large solid timber panels with high in-plane strength and stiffness [5], making it suitable for use as LLRS.

CLT buildings commonly use platform construction with in-plane CLT shear walls as the LLRS. In platform construction, each building storey is constructed sequentially and walls are interrupted by horizontal floor elements. CLT wall elements are generally connected together, to CLT floor elements and to the foundation with mechanical connectors and fasteners similar to those standard LTF connectors. The in-plane behaviour of CLT shear walls in platform construction has been well researched in the last two decades [6]. For example, Dujic et al. [7] tested the in-plane behaviour of CLT shear walls; and subsequent research mainly focused on CLT shear walls using standard LTF connectors [8–12]. It is well recognized that CLT panels behave relatively rigid and the joints are critical to govern the shear wall behaviour. Thus, CLT hold-downs and shear connections have also been extensively studied [13,14]. Depending on the vertical joint details between adjacent CLT wall panels, single, coupled, or combined wall behaviour was observed [11].

As a consequence of a decade of intense research, the design and construction of CLT structures ‘is no longer a domain for early adopters, but is becoming a part of regular timber engineering practice, also in earthquake-prone regions’ [15]. Globally, updates to buildings codes will allow mass timber constructions up to 8-, 12-, and 18-storeys in Australia, Canada, and the United States, respectively [16–18]. In New Zealand, policies such as the “Zero Carbon” Act [19], and Wood First [20,21] are also promoting the use of mass timber construction. In order to realize taller timber structures, enhanced connection solutions are required that meet increased strength and stiffness demands [22]. However, the load carrying capacity of CLT shear walls is only partially exploited when standard LTF connectors are used, which often have only limited capacity [9].

1.2 Capacity Design and Overstrength

In high seismic areas, taller timber structures will require enhanced connection designs to meet not only increased strength and stiffness requirements, but also to develop adequate energy dissipation as ductile joints in capacity design under seismic loading. In capacity design, the overstrength of ductile joints is required and often derived experimentally for timber joints with comparison to current analytical strength models [23]. Further, the inherent flexibility of timber structures compared to reinforced concrete leaves a smaller window to develop this ductility [24]. Current design standards, however, still lack state-of-the-art timber design technology to realize these taller structures [25].

Capacity design requires an understanding of the strength hierarchy among building elements to protect brittle elements by applying overstrength factors derived from ductile elements along the load path [26]. As CLT wall elements behave relatively rigid, joints are often designed as ductile elements and then their overstrength needs to be well understood to protect all non-ductile elements and guarantee system ductility.

In timber structures, the discrepancy between analytical design strength and the 95th percentile of the true strength distribution is generally referred to as overstrength, γ_{Rd}, defined by Jorissen & Fragiacomo [27] as:

$$\boldsymbol{\gamma_{Rd} = \gamma_m \, \gamma_{an} \, \gamma_{0.95} = \frac{F_A}{F_d} \frac{F_{0.05}}{F_A} \frac{F_{0.95}}{F_{0.05}}} \tag{1}$$

where γ_m is the overstrength attributed to material safety factor; γ_{an} is the overstrength due to conservatism in analytical models; $\gamma_{0.95}$ is the overstrength due to the experimental joint strength distribution; F_A is the characteristic strength from analytical models; F_d is the design strength; $F_{0.05}$ is the 5th percentile of strength distribution; $F_{0.95}$ is the 95th percentile of strength distribution. To date, there have been limited studies to establish overstrength factors for timber joints [13,28–31]. Timber joints often contain groups of fasteners, and design codes such as Eurocode 5 [32] introduce an effective number of fasteners to account for a possible group effect. For ductile joints with dowels, these reductions can lead to conservative strength predictions making it difficult to quantify overstrength [30,33]. For STS joints, Tomasi et al. [34] reported no group effect on strength while Hossain et al. [35] provided a conservative recommendation for group effects on both strength and stiffness. In these studies, the possible non-conservative implication of group effect on overstrength was not considered.

1.3 Joint Design with Self-Tapping Screws

Joints with self-tapping screws (STS) can offer superior performance when compared to standardized dowel-type connectors such as nails, bolts or wood screws. STS, manufactured by hardened steel with yield strength up to 1,000 MPa, are the most popular fastener used in mass timber construction, in part due to their ease of installation and flexibility in design [5]. STS -while optimized primarily for axial loading- can offer one reliable solution to meet strength and stiffness demands [36]. Bejtka & Blaß [37] tested STS joints in glued laminated timber by installing inclined STS and developed an analytical strength model that accounts not only for the embedding strength of the timber member and the bending capacity of the STS, but also the withdrawal capacity of the STS and the friction between the members. Their tests showed the increase in strength and stiffness potential with inclined fully threaded (FT) STS.

The stiffness of inclined STS was studied by Kevarinmaki [38] and a stiffness model was proposed for STS installed at 45° in a shear-tension and cross-wise pattern. Subsequent work by Tomasi et al. [34] extended the existing strength model and developed a stiffness model appropriate for any installation angle. The models were compared against experimental monotonic tests in glued laminated timber. The results showed that the strength model was appropriate and that the stiffness model proposed worked if a "single stiffness" approach was adopted, contrary to the system of springs in series approach proposed by Kevarinmaki [38]. The analytical models used to estimate the strength and stiffness of joints with STS are discussed in more detail in Section 4 of this paper. Tomasi et al. [39] also tested combinations of STS installed inclined and STS installed at 90° to the timber grain, simply called 90° STS, in glued laminated timber and reported promising cyclic performance with mixed installations.

The crosswise layup of CLT introduces complexities for joint design. Current design approaches for dowel-type joints in CLT including STS are summarized by Mohammad et al. [40] and Ringhofer et al. [41]. Gavric et al. [29] studied the cyclic performance of 12 different common platform construction STS joints between CLT wall and floor panels. Some tests included in-plane STS spline and lap joints and orthogonal 90° STS joints. It was found that 90° STS joints provided ductile performance in dowel action if recommended spacing and edge distances were followed. The design parameters proposed by Uibel and Blaß [42,43] were appropriate and an overstrength of 1.6 was suggested for the tested STS joints in CLT. Hossain et al. [44] tested butt joints with doubly inclined STS between in-plane CLT panels. The results showed that butt joints, which have a low machining cost, could achieve moderate ductility with a displacement capacity of 8mm under cyclic loading. In-plane CLT lap joints with STS were also studied by considering 90° STS joints, inclined STS joints, and joints with an equal combination of STS in shear and withdrawal [45,46]. The η ratio, i.e. the ratio of STS installed inclined and STS installed at 90° to the timber grain, of 1:1 reported similar findings to Tomasi et al. [39]. With the objective to show that the spatial insertion angle chosen for STS in-plane CLT joints significantly affects the strength, stiffness, and displacement capacity, Loss et al. [47] studied STS in-plane CLT butt joints and compared experimental results to current analytical design models. Satisfactory experimental-analytical agreement was shown for spatially arranged STS strength models but stiffness models were found unsuitable due to the assumptions on individual lateral and axial stiffness components. Increased energy dissipation with increased STS slenderness was also reported [47]. Past research reported that 90° STS act through timber embedment and fastener yielding mechanisms and provide limited stiffness but high displacement capacity, ductility, and energy dissipation. Inclined STS act in withdrawal and provide high strength and stiffness but limited displacement capacity, ductility and energy dissipation. STS joints with η ratio of 1:1 provided promising performance combining high strength, stiffness, ductility, and displacement capacity [39,45–47].

1.4 Cross-Laminated Timber Core-Wall Structures

The feasibility of mass timber core-wall structures has been numerically investigated, either by assuming an orthogonal joint stiffness for a feasibility study [48], or by using small scale inclined STS experimental data as input for orthogonal joint stiffness [49]. There have also been experimental feasibility investigations of post-tensioned CLT core-walls and the results demonstrated CLT core-walls as a viable LLRS with increased strength and stiffness [50]. Figure 1 shows the Cathedral Hill II [51] concept design building plan with a potential core-wall LLRS, to a recently tested 8.6m high C-shaped CLT core-wall at the University of Canterbury [52], and to four options for orthogonal CLT panel joints with STS. The reported C-shaped CLT core-wall results indicated that different levels of partial composite action could be achieved based on different in-plane and orthogonal joint methodologies. STS connections with mixed angle installations for the in-plane and orthogonal joints offered one effective connection solution with significant increases in strength and stiffness when compared to an in-plane CLT LLRS system. The complete experimental programme is introduced Brown et al. [53] which consisted of three post-tensioned CLT shear wall specimens: a single wall, coupled double wall and C-shaped core-wall. A deep understanding of the orthogonal joints is critical for CLT core-wall design considering the composite action.

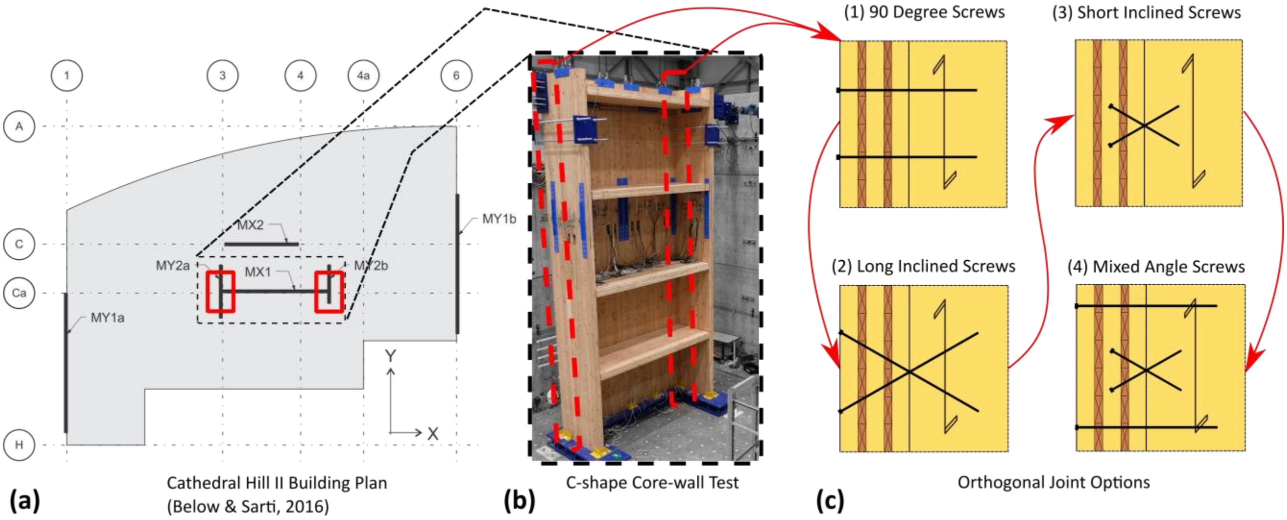

Figure 1: (a) Cathedral Hill II concept design [51] *(b) C-shape core-wall test [52] (c) orthogonal joint options with STS*

1.5 Objective of research

Past experimental work on STS joints in CLT has focussed on common in-plane joints with relatively smaller fasteners (up to ø10mm x 200mm) and thin 3- or 5-ply CLT panels. Past orthogonal CLT panel joint tests with STS were limited to 90° installation angles [29]. As taller timber buildings will require thicker (5-, 7-ply or greater) CLT panels with larger diameter STS, experimental testing to verify performance is required. While the use of mixed angle STS with an η of 1:1 has shown promising performance for seismic design [39,45,46], little work has quantified the impact of inclined to 90° STS η ratio on the joint performance.

The primary objective of this study is to evaluate the performance of orthogonal CLT panel joints with varying mixed angle STS combination ratios, η. These joints are of particular interest for their potential to develop composite action between orthogonal CLT wall panels, which could transform conventional in-plane CLT

LLRS to a core-wall structure with enhanced lateral strength and stiffness. In this study, a total of 59 CLT orthogonal joint tests were performed in 9 different configurations with varying STS η ratio under monotonic and cyclic loading. The different joint configurations were chosen to evaluate which mixed angle STS joint combination could provide enhanced seismic performance and efficiency. The secondary objectives are to compare current analytical strength and stiffness models with the experimental results and to evaluate overstrength. Input parameters for the analytical models are based on both current STS design documents and experimental data from baseline STS withdrawal and lateral load tests.

2 Experimental programme

2.1 Specimen Description

The test programme is shown in Table 1. A total of 59 joint specimens were tested in nine series with different connection configurations. In labelling each test series, the number indicates the quantity of screws installed in the joints and S, ST, SC, and X indicate different installations: S = 90° STS; ST = shear-tension STS; SC = shear-compression STS, and X = cross-pattern STS (i.e., a combination of shear-tension and shear-compression STS), respectively. Note the test series 16X-400 label is unique and used 16 STS 400mm long, installed in cross-pattern. Three series (2S, 8ST, 8SC) were tested under monotonic (M) loading only, the other six series were tested under both M and reversed cyclic (C) loading. The number of replicates for monotonic tests was three except for the 2S test series which had five replicates; the number of the replicates for cyclic tests was five.

Each test series was designed to verify current design models for mixed angle STS as applicable to orthogonal CLT joints. The test programme allowed to assess the performance of orthogonal CLT panel joints with varying mixed angle STS combination ratios. With series 2S, 8ST, 8SC, and 16X, the applicability of existing analytical models to estimate the load-carrying capacity was assessed. By comparing series 16X-400 and 16X, the influence of STS embedment length on strength, stiffness, and failure mode was investigated. Comparing series 16X and 16X+16S (combination of 90° STS and inclined STS) allowed for verification of the increase in displacement capacity and ductility. Finally, series 12X, 12X+4, and 12X+6 aimed to determine the impact of 90° STS on strength, displacement capacity, ductility, stiffness, and energy dissipation. STS slenderness, $\lambda = L/d_c$, where L and d_c are the STS length and core diameter, varied from 40 to 80 by considering STS of different L and d_c.

The specimens consisted of 5-ply 175mm thick CLT with a layup of 45/20/45/20/45 and 7-ply 275mm thick CLT with a layup of 45/35/35/45/35/35/45, herein simply referred to as CLT5 and CLT7, respectively. The Douglas-fir lamella were graded SG8 with average Modulus of Elasticity of 8 GPa according to NZS3603 [54]. After testing, a small piece was removed from each specimen and oven dried to determine density and moisture content. The CLT specimens had an average moisture content of 11%, and the mean and characteristic densities were ρ_{mean} = 462 kg/m^3 and ρ_k = 422 kg/m^3 for CLT5 specimens and ρ_{mean} = 457 kg/m^3 and ρ_k = 417 kg/m^3 for CLT7 specimens respectively.

SPAX [55] fully threaded (FT) ø8mm STS were used for the CLT5 specimens and FT ø12mm STS were used for the CLT7 specimens. The STS length varied for inclined STS and STS installed at 90°. In series 16X-400 the inclined STS length was longer than 90° STS in a similar manner as past research [34,46,56]. However, in all other series to ensure screw withdrawal failure occurred the inclined STS were shorter than 90° STS. The η ratio, i.e. the ratio between inclined STS and STS installed at 90°, varied from 1:0, 3:1, 2:1, 1:1, and 0:1 in the joints. Shear-tension and shear-compression screws were both considered inclined STS. The η ratio of 0:1 indicated that only 90° STS were used and the η ratio of 1:0 indicated that only inclined STS were used. The η ratios of 3:1, 2:1 and 1:1 indicated the inclined STS to 90° STS ratio. For example, an η ratio of 3:1 meant that for three inclined STS there was one 90° STS. Changing the η ratio accordingly from 1:0, 3:1, 2:1 to 1:1 was defined as decreasing the η ratio, and hence increasing the amount of 90° STS in the joint.

Table 1: Experimental Test Programme

Series	**Load Type**	**Repl.**	**CLT**	**Inclined STS**			**90° STS**			**Mixed Angle**
				Type	**λ**	**Qty.**	**Type**	**λ**	**Qty.**	**STS Ratio (η)**
2S	M	5	CLT5	-	-	-	ø8x350	70	2	0:1
8ST	M	3	CLT5	ø8x200	40	8	-	-	-	1:0
8SC	M	3	CLT5	ø8x200	40	8	-	-	-	1:0
16X-400	M	3	CLT5	ø8x400	80	16	-	-	-	1:0
	C	5	CLT5	ø8x400	80	16	-	-	-	1:0
16X	M	3	CLT5	ø8x200	40	16	-	-	-	1:0
	C	5	CLT5	ø8x200	40	16	-	-	-	1:0
16X+16S	M	3	CLT5	ø8x200	40	16	ø8x350	70	16	1:1
	C	5	CLT5	ø8x200	40	16	ø8x350	70	16	1:1
12X	M	3	CLT7	ø12x350	47	12	-	-	-	1:0
	C	5	CLT7	ø12x350	47	12	-	-	-	1:0
12X+4S	M	3	CLT7	ø12x350	47	12	ø12x550	74	4	3:1
	C	5	CLT7	ø12x350	47	12	ø12x550	74	4	3:1
12X+6S	M	3	CLT7	ø12x350	47	12	ø12x550	74	6	2:1
	C	5	CLT7	ø12x350	47	12	ø12x550	74	6	2:1

Figure 2 shows the test specimens and joint details of all test series. Figure 2a and Figure 2b provide isometric views and the dimensions for the CLT5 and CLT7 specimens. The Ø8mm and Ø12mm STS were installed into Ø5mm and Ø7mm predrilled holes, respectively, to 70% of the screw length with jigs to ensure correct alignment. Each joint specimen had three CLT panels: two side panels and one middle panel. The two side panels were connected to the middle panel with STS installed in a symmetrical layout such that each specimen had two orthogonal joints. Figure 2c - Figure 2k show one joint and half of a test specimen to provide details for each STS layout including the η ratio. The monotonic loading direction is indicated for the 8ST and 8SC test series to show the shear-tension and shear-compression STS respectively. The fastener spacing followed the product ETA [55]. In all test series except 16X-400, the inclined STS were countersunk into the side panels to ensure equal embedment length of the screw into the side panel and the middle panel.

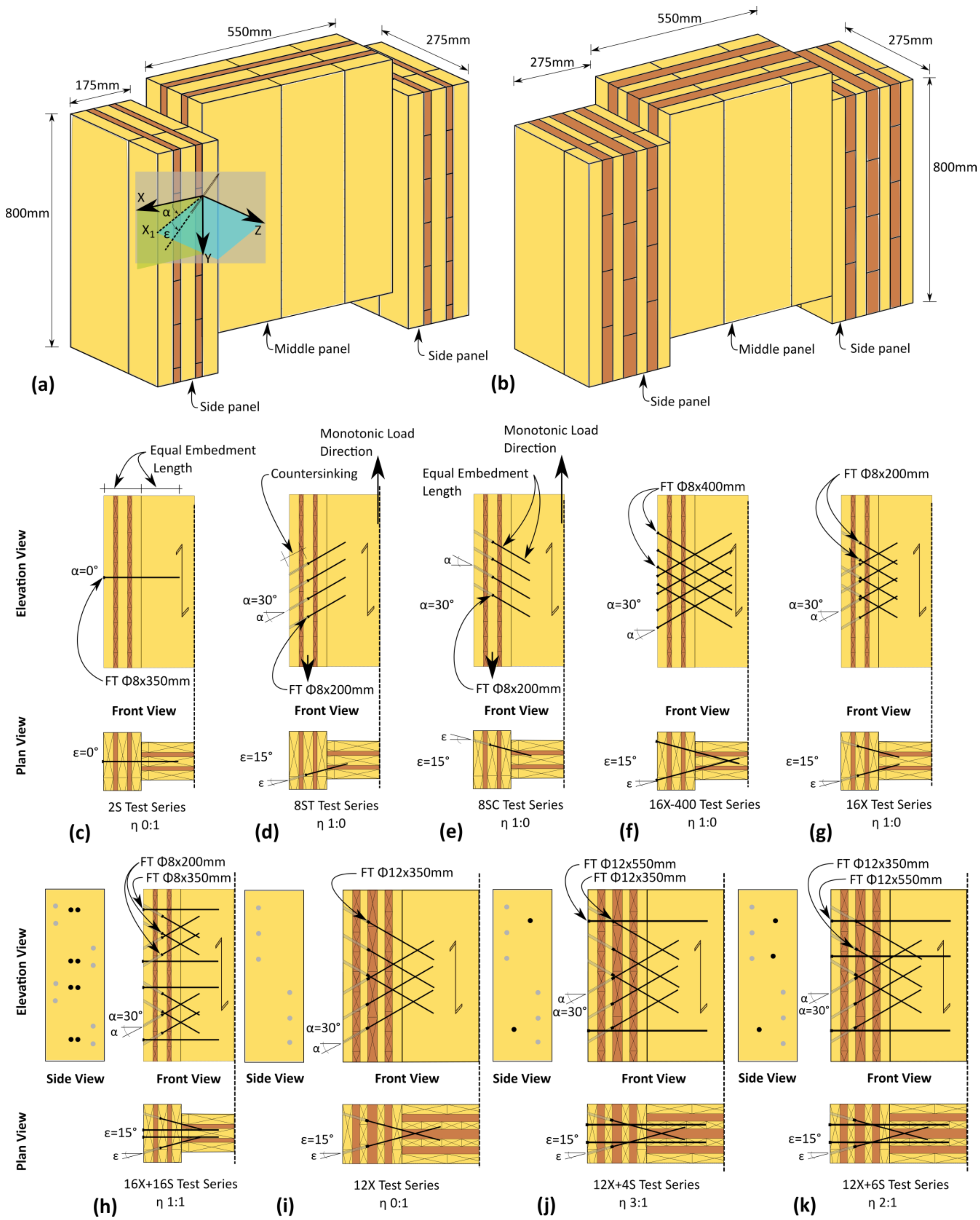

Figure 2: (a) CLT5 isometric (b) CLT7 isometric (c) 2S test series (d) 8ST test series (e) 8SC test series (f) 16X-400 test series (g) 16X test series (h) 16X+16S test series (i) 12X test series (j) 12X+4S test series (k) 12X test series

In these test series, the inclined STS embedment length was chosen based on single STS withdrawal studies [57] so that the withdrawal strength was sufficiently greater than the STS tensile strength to promote STS withdrawal failure and minimize brittle STS tensile failure. All inclined STS were installed at $\alpha = 30°$ and $\varepsilon = 15°$ to create a double angle. 90° STS did not have a double angle. For inclined STS, a double angle was implemented for the following reasons: (1) the product ETA [55] requires a minimum angle to the grain of 15° for withdrawal capacity; (2) the general embedding strength formulation could be used which is significantly higher than the reduced formulation for STS installed parallel to the CLT plane as per product ETA [55]; (3) significant homogenization is found when STS penetrate more layers [58]; and (4) for an actual core-wall application, the orthogonal joint would be subjected to bi-directional loading and a double angle would provide optimized axial STS loading in either direction.

2.2 Methods

Figure 3 shows the test setup. A 700 kN capacity hydraulic ram with a load cell was clamped to the middle CLT panel of the joint specimen. The two side CLT panels were fully restrained by steel plates and 4-M20 Grade 8.8 threaded rods [59]. Horizontal in-plane movement was also restrained by two sets of steel plates with 4-M36 Grade 8.8 threaded rods placed at the top and bottom of the specimen. Out-of-plane translation and rotation was prevented by a horizontal steel beam with rectangular hollow section that was bolted to the reaction frame.

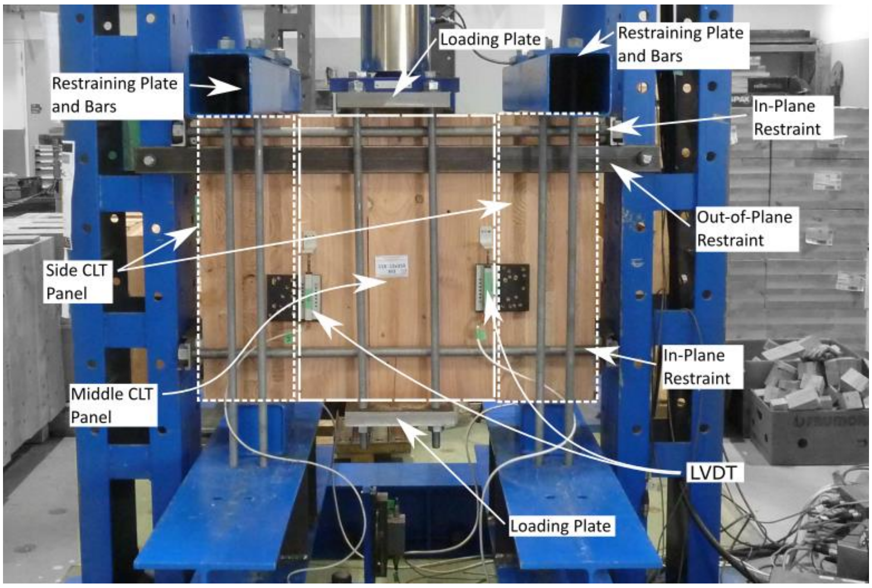

Figure 3: Overall test set-up

Figure 4 shows the instrumentation used in the testing. Relative displacement between the middle and outer CLT panels was measured with 100mm linear variable displacement transducers (LVDTs) at two points on each shear plane for a total of four measurements. The average joint slip was determined from the four measurements. Out-of-plane displacement was also measured at two points.

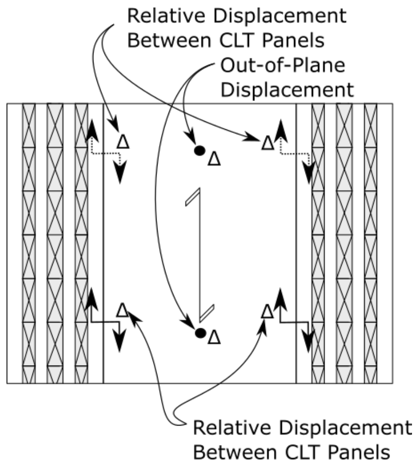

Figure 4: Specimen instrumentation - CLT7 joint specimen shown

Test series 2S, 8ST and 8SC were tested under monotonic loading only following EN 26891 [60]. For these test series if a maximum strength was not reached the joint slip was limited to 15mm following EN 26891 [60]. For the remaining test series, three monotonic tests were performed first to determine the average yield displacement, Δ_y, that was used as the reference displacement to define the cyclic loading protocol as per EN 12512 [61]. One cycle amplitude at $0.25\Delta_y$ and $0.5\Delta_y$ were performed followed by three cycle amplitudes at $0.75\Delta_y$, $1.0\Delta_y$ $2.0\Delta_y$, $4.0\Delta_y$, and then increasing multiples of $2.0\Delta_y$ ($6.0\Delta_y$, $8.0\Delta_y$, etc.) until failure as defined by EN 12512 [61] and explained later. The monotonic loading rate was between 3-6mm/min for a total test time of 10 to 15min as per EN 26891 [60] and the cyclic loading rate was between 12-18mm/min as per EN 12512 [61]. The results were analysed as per EN 12512 [61] to determine the yield strength F_y, maximum strength F_{max}, and ultimate strength F_u, the corresponding yield displacement Δ_y, displacement at maximum strength Δ_{Fmax}, ultimate displacement Δ_{Fu}, and the elastic stiffness, k. The elastic stiffness was calculated for the range of the load-slip curve between 10% and 40% F_{max} as per EN 26891 [60]. Herein, the displacement capacity is synonymous to the ultimate displacement defined as the displacement at which F_u occurred, which is the post-peak load at 80% of F_{max}. While EN 12512 [61] assesses the ultimate strength F_u to a maximum slip of 30mm, in 16X+16S, 12X+4S and 12X+6S test series slips greater than 30mm were recorded and they are presented to illustrate the impact of the η ratio on joint performance. Energy dissipation properties were derived in terms of equivalent viscous damping following EN 12512 [61]. Ductility, μ, is reported as it is often defined as a ratio of Δ_{Fu} to Δ_y, as shown in Eq. **2** [27].

$$\boldsymbol{\mu} = \frac{\Delta_{\boldsymbol{Fu}}}{\Delta_{\boldsymbol{y}}} \tag{2}$$

Following the recommendations by Smith et al. [62], the joint was defined as low ductility (LD) for $\mu<4$, as moderate ductility (MD) for $4\leq\mu\leq6$, and as Ductile (D) for $\mu> 6$.

3 Experimental Test Results and Discussion

3.1 Overview

Table 2 provides a summary of joint performance parameters as mean, X_m, with coefficient of variation (CV), for each test series. Similar to the results reported by Tomasi et al. [34], ultimate loads were not observed in both 2S and 8SC test series groups even at large joint slips. Thus, as per EN 26891 [60] the ultimate slip was limited to 15mm. For the 16X+16, 12X+4, and 12X+6 monotonic test series, F_{max} is reported as the average load at the first peak on the load-slip curve. In the mixed angle test series under monotonic loading, the load kept increasing after an initial drop at the first peak and even surpassed the first peak load. The load at the first peak is required in Section 4 for comparison to analytical models and to derive cyclic overstrength.

Table 2: Test summary of joint performance factors

Series		Fy		Fmax		Fu		Δy		Δmax		Δu		K		μ	
		X_m	CV	X_m	CV	X_m	CV	X_m	CV	X_m	CV	X_m	CV	X_m	CV	X_m	CV
		kN	%	kN	%	kN	%	mm	%	mm	%	mm	%	kN/mm	%	-	%
2S	M	7	12	7[1]	-	18	15	6.0	20	6[1]	-	15[2]	-	0.8	14	-[2]	-
8ST	M	121	3	138	2	110	1	2.7	30	5.8	10	11.0	16	45	24	4.2	13
8SC	M	24	13	34[1]	-	34	6	0.7	22	6[1]	-	15[2]	-	33	23	-[2]	-
16X-400	M	191	2	208	4	167	4	3.8	23	5.9	10	7.1	19	49	19	1.9	15
	C	177	9	202	4	169	7	2.6	15	5.0	7	5.6	11	69	16	2.3	30
16X	M	120	30	153	20	122	20	1.7	35	6.3	29	11.1	16	69	26	7.3	52
	C	134	8	165	5	132	5	1.6	27	5.0	9	7.3	12	83	21	4.9	18
16X+16S	M	190	2	244[1]	4	251	4	1.9	12	6[1]	4	26.9	14	92	18	14.4	10
	C	179	6	238	3	190	3	1.7	14	11.0	65	21.8	27	107	15	14.4	24
12X	M	188	4	219	6	176	6	2.4	36	5.8	18	16	18	75	27	7	16
	C	186	11	243	7	195	7	1.6	13	5.7	12	11.6	21	110	8	7.9	33
12X+4S	M	226	11	290[1]	8	277	20	2	8	8[1]	7	50.2	32	103	3	25	37
	C	236	7	309	5	247	5	1.7	7	6.6	11	13	9	126	5	7.8	16
12X+6S	M	246	8	314[1]	6	308	6	2.2	32	8[1]	4	49.3	4	102	25	23.5	29
	C	215	6	314	5	251	5	1.3	18	9.4	13	24.1	29	151	12	20.2	41

Notes: 1 indicates Fmax chosen as load at first peak for analytical comparison
2 as per EN 26891, Δu = 15mm and μ not stated as a maximum load was not reached

Figure 5 shows the experimental monotonic and hysteresis curves for all test specimens which included two joints. The force represented the total applied load and the relative joint displacement, slip, was derived by averaging the data measured from four LVDTs. It was found that the curves of the replicates in each series were consistent. Therefore, for each test series, one representative monotonic load-slip and one representative cyclic load-slip curve are provided. The monotonic-load slip curves for the inclined STS show that when tensile screw failure was avoided, the joint had stable post-peak performance that varied between test series due to the η ratio. With only inclined STS (η of 1:0), limited displacement capacity was observed. However, the post-peak displacement capacity was significantly increased by adding 90° STS with the η ratio reduced.

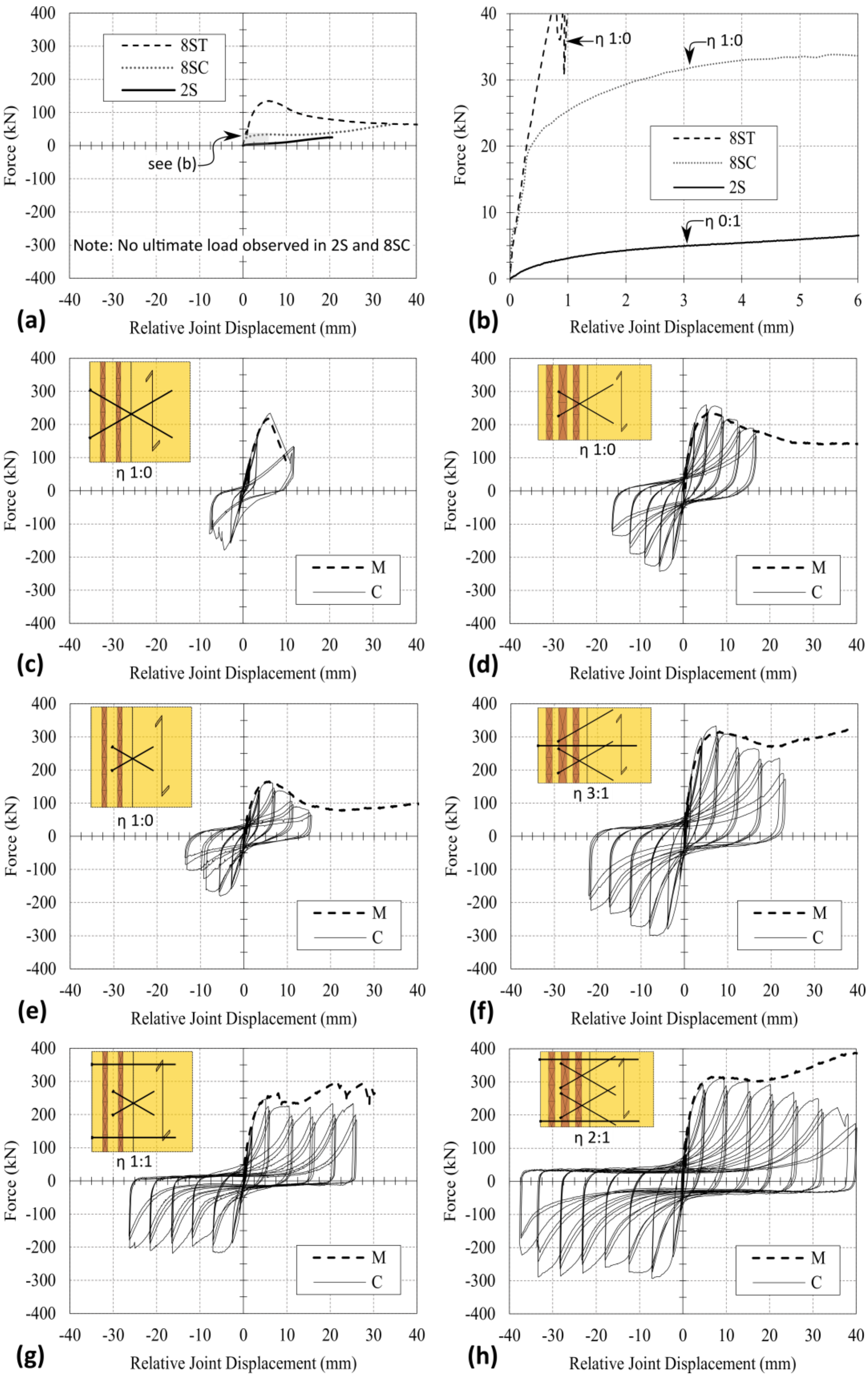

Figure 5: Monotonic and cyclic load-slip curves by test series; (a) and (b) 2S, 8ST, 8SC, (c) 16X-400, (d) 12X, (e) 16X, (f) 12X+4S, (g) 16X+16S, (h) 12X+6S

The cyclic load-slip curves showed typical pinching behaviour and stable response in all series other than 16X-400, when brittle screw tensile failure occurred. With the addition of 90° STS the displacement capacity increased and the pinching behaviour was more pronounced. Other than for series 16X-400, F_{max} was within 10% on average between the positive and negative cycles. The displacement capacity was less consistent between positive and negative cycles of each test.

3.2 Failure Modes

Figure 6 shows typical failure modes for series 16X, 16X+16S and 12X after testing by showing the side and middle panel respectively. Figure 6a - Figure 6f show plastic embedment deformation and the length is indicated at each STS location in mm. Figure 6c and Figure 6d show the longest plastic embedment deformation lengths, indicative of the test series large displacement capacity and the most STS tensile failure as well. Significant plastic embedment deformation is shown by the pronounced pinching behaviour in Figure 5g and Figure 5h. Figure 6e shows STS yielding that occurred with each STS removed from the joint specimen. Series 16X-400 had brittle tensile failure of the screws on one shear plane which propagated in a zipper like effect. This is shown by the sudden load drop in Figure 5c. These tests were characterised with low ductility in both monotonic and cyclic loading. The reduced embedment length in series 16X compared to 16X-400 led to a more gradual screw withdrawal as the dominating failure mode, as shown in Figure 5e (series 16X) and Figure 5d (series 16X-400). For the remaining test series, the shortened length of the inclined STS ensured gradual STS withdrawal failure mode. Under monotonic loading tensile screw failure was avoided in most instances and the load increased at larger slips due to the significant rope effect as observed by Tomasi et al. [34]. Under cyclic loading, in some instances tensile screw failure occurred at larger slips but a sudden load drop was avoided. In the mixed angle screw test series, a more complex failure mode similar to that reported by Hossain et al. [45] was observed. The inclined screws provided high initial stiffness. Once screw withdrawal started, a small load drop was observed but the 90° screws became more engaged to carry the load. Under cyclic loading with increased slips, STS tensile failure occurred and the load dropped significantly. However, a progressive zipper-like failure as observed in series 16X-400 did not occur with mixed angle screws and the joint continued to sustain the load. The η ratio influenced the shape of the load slip-curve and failure mode. Figure 5f with η of 3:1 had similar behaviour to the test series in Figure 5d and Figure 5e with η of 1:0. However, Figure 5h with η of 2:1 had similar behaviour to the test series in Figure 5g with η of 1:1, which had been studied for in-plane CLT joints [45,46]. With both decreasing η and increased quantity of screws in the joint, the tensile failure of an individual screw had a lesser effect on the overall joint behaviour.

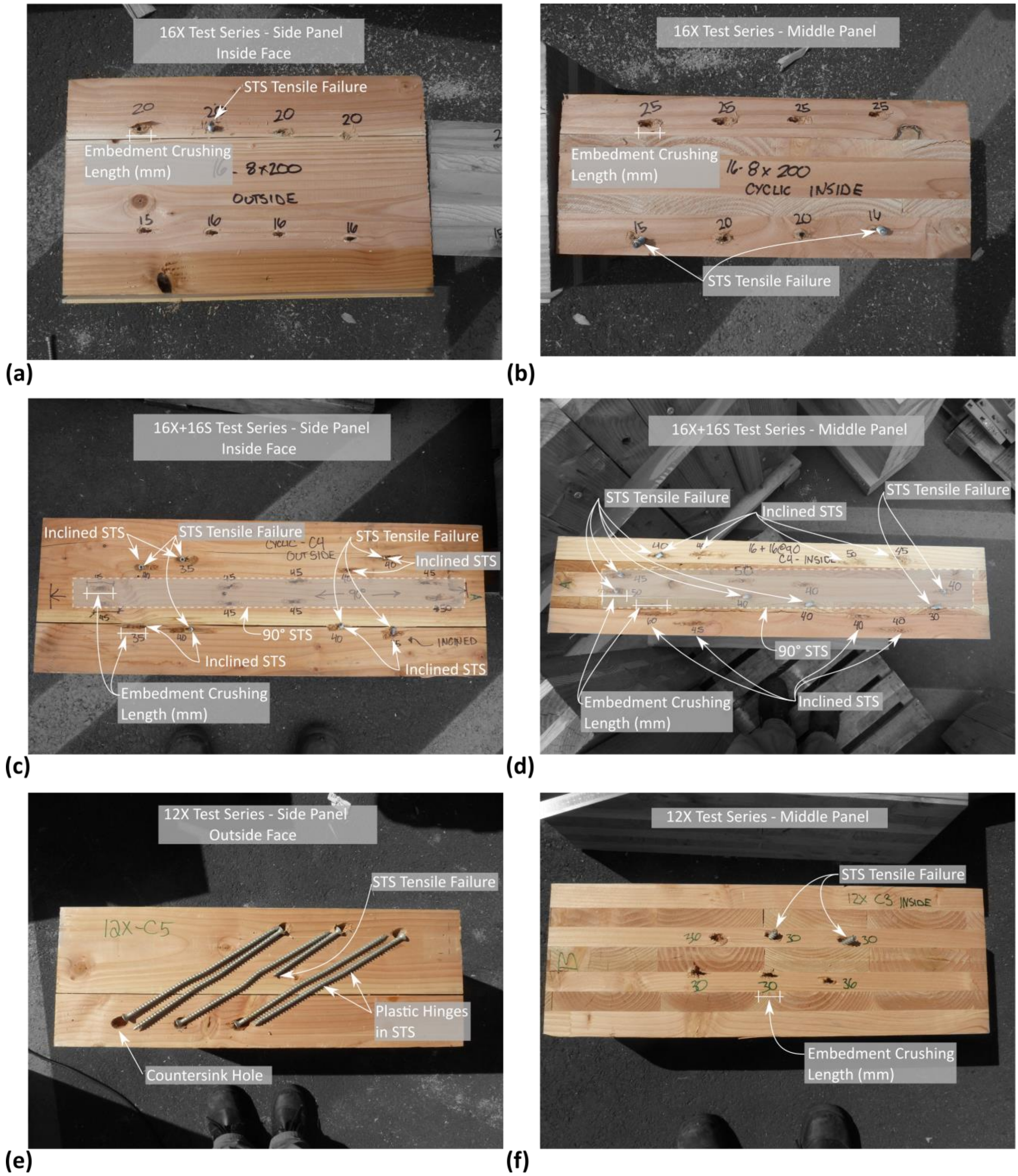

Figure 6: After test specimen photos: (a) 16X side panel (b) 16X middle panel (c) 16X+16S side panel (d) 16X+16S middle panel (e) 12X side panel (f) 12X middle panel

3.3 Strength

As shown in Table 2, inclined STS joints had significantly higher maximum strength, F_{max}, than 90° STS joints given the specific parameters tested. On a per screw basis and neglecting a possible group effect, F_{max} was approximately five times higher in 8ST test series than 2S test series when considered at the 15mm slip limit. This agrees with past reported research which indicated inclined STS can provide increased strength [34,45–47]. F_{max} in test series 16X was less than 16X-400 due to shorter embedment length. The load-carrying capacity was also less than the superposition of 8ST and 8SC, which indicated that assuming the friction term balanced and was zero in a cross-wise configuration as per Bejtka & Blaß [37] was appropriate in this instance. A progressive increase in F_{max} was observed from series 12X, to 12X+4S, and then to 12X+6S, indicating that the 90° screws contributed to the strength. In all test series except 16X, the CV was notably small (< 8%) and decreased with decreased η and increased screw quantity. The higher CV for F_y (around 9%) when compared to the CV for F_{max} (around 5%) can be attributed to the sensitivity of the method to analyse the load-slip curve [63]. That the CV decreased with decreased η and increased screw quantity indicated the effectiveness of using mixed angle screw combinations, and the importance of testing large multi-fastener joints (up to 16 screws per joint and 32 screws per specimen) to represent actual applications. On average, the ratio of cyclic F_{max} to monotonic F_{max} was 1.04 which was contrary to previous findings by Hossain et al. [45].

3.4 Displacement Capacity and Ductility

The displacement capacity, synonymous to the ultimate displacement or 15mm limit for monotonic specimens which did not reach maximum load, and ductility increased significantly with a maximum η ratio of 2:1. Firstly, the displacement capacity of series 16X+16S with η=1:1 was three times larger than for series 16X, which confirmed previous findings for in-plane mixed angle STS CLT joints [45,46]. It was found that a minimum number of 90° STS, herein half the number of inclined STS, were required to provide significant influence on joint behaviour. Cyclic ductility was unchanged between series 12X and 12X+4S which indicated that the η ratio of 3:1 was too large and the influence of 90° screws was not significant. However, the series with η of 2:1 (12X+6S) and 1:1 (16X+16S) had high displacement capacity greater than 20mm and cyclic ductility greater than 14, respectively, demonstrating that 90° screws significantly contributed for such ratios. This indicated that a maximum η of 2:1 could be recommended to achieve enhanced joint behaviour. It should be noted that if gradual screw withdrawal of inclined STS was the governing failure mode, moderate ductility was achieved, in agreement with past studies [44,47]. Though, with an η of 1:0 the cyclic displacement capacity is limited and less than 12mm. STS slenderness, $\lambda = L/d_c$, impacted displacement capacity and ductility. When comparing series 12X to 16X, cyclic displacement capacity and ductility increased by a factor of 1.5 with increased λ to 47 from 40 even with larger diameter and fewer STS in the 12X series. Past work by Loss et al. [47] and Sullivan et al. [46] also had increased ductility with increased λ. STS slenderness as an influencing parameter on STS joint performance will be discussed further and the results indicated that slenderness may be a more representative parameter irrespective of STS diameter which had been reported in past work [46]. In all test series, the displacement capacity and ductility were lower under cyclic loading compared to monotonic loading. Displacement capacity and ductility were 35% and 15% lower on average respectively. The yield displacement was also 20% smaller on average under cyclic loading, but was minimally affected by changing η.

3.5 Stiffness

The stiffness of inclined STS in ST, SC and X configuration test series was significantly higher than the 90° screws as expected. For series 2S, upon evaluating the elastic portion of the curve in a similar manner to Gavric et al. [29], the derived elastic stiffness was 1.8kN/mm/screw and almost 5 times less than series 16X. While this comparison neglects a possible group effect, it agrees with past reported research which indicated inclined STS provide increased stiffness [34,45–47]. It should be noted that as per EN 12512 [61], the stiffness for 2S was only 0.4kN/mm/screw, but this was significantly influenced by the shape of the load-slip curve and deemed not representative for comparative purposes in this instance. The joint stiffness also increased with decreasing η which indicated that 90° screws impact stiffness. For instance, the progressive increase in cyclic stiffness from series 12X, to 12X+4S, and then to 12X+6S was 110, 126, and 151 kN/mm. Increased STS slenderness, λ, appeared to influence and decrease joint stiffness. The stiffness of series 16X (λ=40) was 1.2 times higher than that of series 16X-400 (λ=80) which is contrary to the values calculated by the product approval [55], as the STS embedment length in 16X was approximately half that in 16X-400. In the product approval [55] stiffness increases linearly with embedment length. A comparison between series 8ST and 8SC with 16X indicated that there was a contribution from friction to stiffness for shear-tension STS in agreement with past reported work [34,47]. The cyclic stiffness was on average 1.3 times higher than the monotonic stiffness, which could in part be due to the faster cyclic loading rate.

3.6 Energy Dissipation

Energy dissipation was evaluated in terms of equivalent viscous damping, ξ, for the first and third cycle of the load-slip curve at each displacement amplitude. The results are presented as the averages of the replicates of the test series. Figure 7 reports ξ for each displacement amplitude cycle up to the limit of post-peak load at 80% of F_{max} in a similar manner to Loss et al. [47]. The results indicated that ξ was directly linked to the associated failure mode. In all test series, the initial increase in ξ at early displacement cycles is indicative of ST and SC screws loaded in withdrawal which have low initial energy dissipation capacity due to high elastic stiffness [44]. Steel tensile failure in 16X-400 resulted in the lowest ξ as expected. For the remaining test series, ξ reached its peak in the two or four times yield displacement amplitude cycles. The increased ξ was due to gradual withdrawal of STS, timber embedment deformation, and STS bending yielding deformation. With decreased η, at large displacement ξ gradually decreased and the difference between ξ_{1st} and ξ_{3rd} was more significant which is typical in dowelled joints or STS installed at 90° with pinched hysteresis loops [29].

Previous testing by Loss et al. [47] reported increased ξ to 8% with increased λ from 23 to 30 and noted this positive correlation. In this instance, the average ξ at maximum load was 10% with λ of 40 and 47, which is 1.25 times higher than ξ reported by Loss et al. [47] with lower λ. The ξ was found to be similar to values reported by Tomasi et al. [39] with a mixed angle STS installation joint and λ of 41. While increased λ may increase energy dissipation capacity, λ of inclined screws should be limited to avoid STS tensile failure.

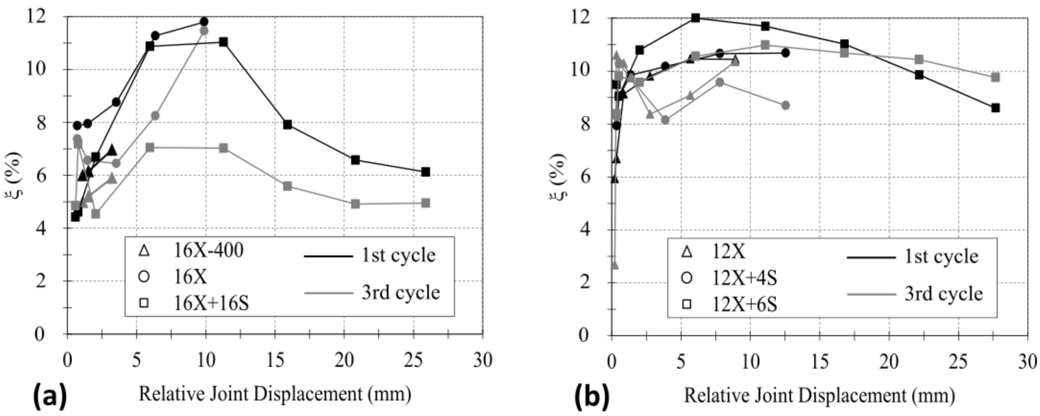

Figure 7: Equivalent Viscous Damping of each test series: (a) CLT5 specimens (b) CLT7 specimens

4 Analytical Models and Comparisons with Experimental Results

4.1 Experimental Considerations for Models

For all inclined STS test series, the angle $\varphi_{/\!/} = \varphi$ between the screw axis and the grain of the longitudinal CLT layer is related to the screw installation angles α = 30° and ε = 15°, calculated by Eq. **3**.

$$\cos \boldsymbol{\varphi} = \cos \boldsymbol{\varepsilon} \sin \boldsymbol{\alpha} \tag{3}$$

The angle between the screw axis and the grain of the longitudinal and cross CLT layer is $\varphi_{/\!/}$ and $\varphi_{\perp}$ respectively. The angle between the embedment force and the grain of the longitudinal and cross layer is $\theta_{/\!/}$ and $\theta_{\perp}$ respectively. As such, for design purpose the design angles for the longitudinal and cross layer were $\varphi_{/\!/} = \varphi = 61°$, $\varphi_{\perp} = 33°$, and $\theta_{/\!/} = \theta = 29°$ for all test series, as shown in Figure 8. Table 3 provides a summary of key STS properties required for analytical models.

Table 3: Test series STS details

Series	STS Name	d mm	l mm	d_c mm	l_t (min) mm
16X-400	Ø8x400	8	400	5	375
2S, 16X+16S	Ø8x350	8	350	5	325
8ST, 8SC, 16X, 16X+16S	Ø8x200	8	200	5	185
12X+4S, 12X+6S	Ø12x550	12	550	7.4	525
12X, 12X+4S, 12X+6S	Ø12x350	12	350	7.4	325

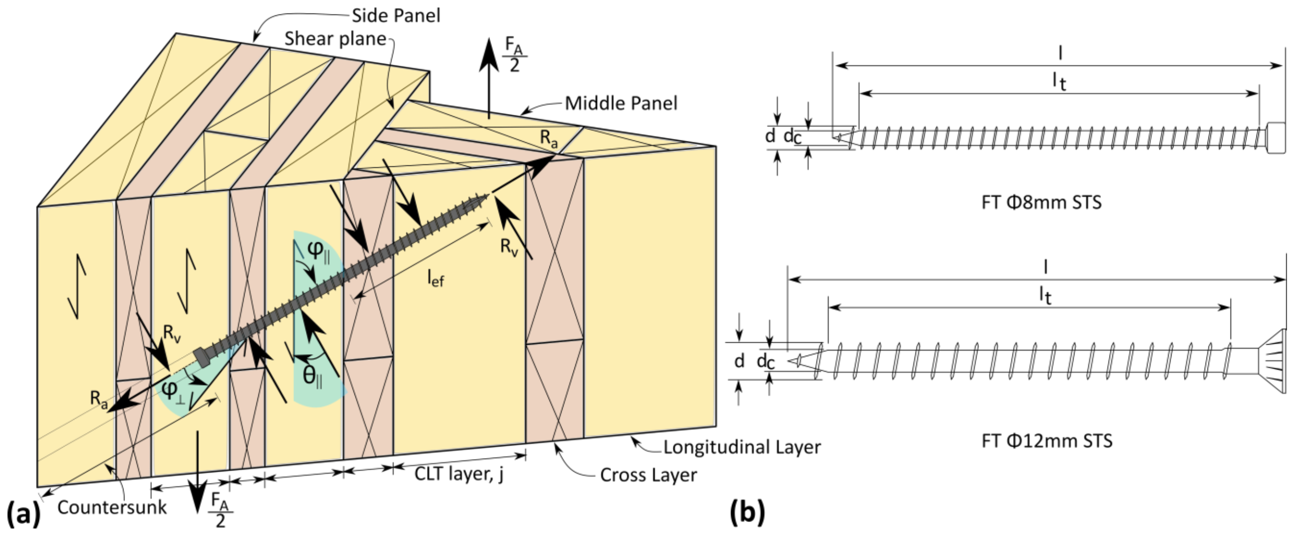

Figure 8: (a) Isometric of shear-tension Ø8mm STS in CLT5 (b) key parameters for STS

4.2 Strength Model

The analytical strength model developed by Bejtka and Blaß [37] with extensions by Jockwer et al. [64] was adapted herein for orthogonal joint design. As STS joint design is not covered by many design standards including New Zealand Timber Structures Standard NZS3603 [54], design guidance within the SPAX ETA [55] was used to determine the withdrawal strength, fastener bending yield moment, and embedment strength component properties for the analytical model because there are differences between different STS ETAs [36]. While current design codes guide designers to a ductile joint by introducing certain factors such as an effective number of fasteners, n_{ef}, Dorn et al. [33] reported this can lead to conservative strength predictions for ductile joints. This makes it hard to quantify the overstrength due to conservatism in analytical models, γ_{an}, and was therefore not considered herein. Accordingly, the withdrawal strength parameter, f_1, is 12.0 and 11.0MPa for the Ø8mm and Ø12mm STS respectively, and the bending yield moment, M_y, and embedment strength, $f_{h,\varphi}$, are calculated by Eq. **4** and Eq. **5**.

$$\boldsymbol{M_y = 0.15(600)d^{2.6}} \tag{4}$$

where d is the outer thread diameter. The embedment strength for inclined screws, $f_{h,\varphi}$, is determined as:

$$\boldsymbol{f_{h,\varphi} = \frac{0.082\rho_k(1-0.01d)}{(2.5\cos^2\varphi + \sin^2\varphi)(k_{90}\sin^2\theta + cos^2\theta)}} \tag{5}$$

where ρ_k is the characteristic CLT density, $k_{90} = 1.35\text{-}0.015d$, and $\varphi = \varphi_{//}$ and $\theta = \theta_{//}$ as defined above as the angles to longitudinal CLT layer grain direction. For 90° STS in all test series, the embedment strength was $f_{h,S}=20d^{-0.5}$ in the middle panel as the STS was installed parallel to the plane of CLT. With reference to Figure 9, for the orthogonal joint specimen, the side and middle panel, $i = sp$ *or* mp, strength is determined separately and the minimum governs the specimen capacity as per Eq. **6**.

$$F_{A,specimen} = 2 * min\begin{cases} F_{A,SIDE\ PLATE} \\ F_{A,MIDDLE\ PLATE} \end{cases} \tag{6}$$

where the factor 2 accounts for both sides of the symmetrical specimen to determine the overall specimen capacity. In all instances, the side panel strength governed the capacity due to the lower rolling shear strength of the 45mm layer required for Eq. **12**, which will be discussed further.

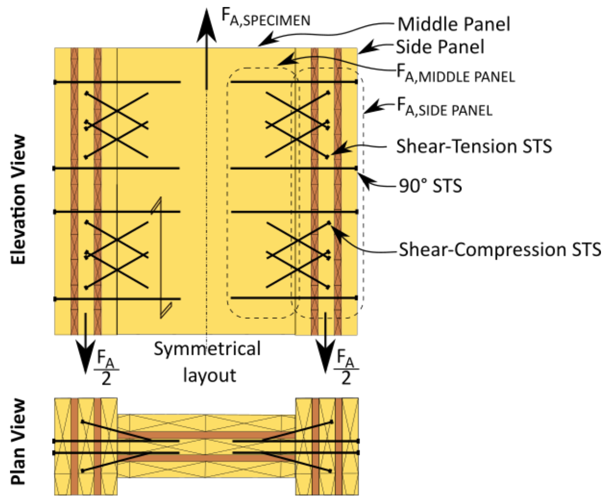

Figure 9: Strength calculation illustrated by 16X+16S specimen

For a 90° STS acting in dowel action as in the 2S series, the Johansen equations of Eurocode 5 [32] with consideration for the rope effect are considered as:

$$F_{A,S,i} = R_{v,i} + min\begin{cases} R_{a,i}/4 \\ R_{v,i} \end{cases} \tag{7}$$

where $R_{v,i}$ is shear strength in dowel action and $R_{a,i}$ is the axial strength determined in Eq. **9**. The slenderness of the STS ensures plastic hinges will develop such that $R_{v,i}$ is:

$$R_{v,i} = \sqrt{\frac{2\beta}{1+\beta}}\sqrt{2M_y d_{ef} f_{h,\varphi,i}} \tag{8}$$

with M_y as defined before, $d_{ef} = 1.1d_c$ where d_c is the screw core diameter and $f_{h,\varphi,i}$ as defined before. $\beta = f_{h,\varphi,mp}/f_{h,\varphi,sp}$, is the ratio between embedment strengths on the screw middle panel side and screw side panel side. In the instance of ST and SC STS β = 1. The determination of $R_{a,i}$ was as per ETA [55] as the minimum of either the withdrawal strength or the STS tensile strength:

$$\mathrm{R_{a,i}} = \min\left(\frac{f_1 \mathrm{dl_{ef}}}{1.2\cos^2\varphi + \sin^2\varphi}\left(\frac{\rho_k}{350}\right)^{0.8};\ 17,000\ (\emptyset 8mm), 38,000\ (\emptyset 12mm)\right) \tag{9}$$

where f_1, d, and $\varphi = \varphi_{/\!/}$ are as defined before, and l_{ef} is the screw thread length (mm) in each CLT panel side, which was half the screw thread length ($l_t/2$). For each side and middle panel the withdrawal strength determination, $R_{a,i}$, is the sum of each component determined for each CLT layer, j, penetrated considering both l_{ef}, $\varphi_{\parallel}$ and $\varphi_{\perp}$ with reference to Figure 8. For the shear-tension (ST) STS, the strength is determined as:

$$\boldsymbol{F_{A,ST,i}} = \mathbf{R}_{\boldsymbol{a,i}}\ (\boldsymbol{\psi}\ \mathbf{sin}\,\boldsymbol{\varphi} + \mathbf{cos}\,\boldsymbol{\varphi}) + \boldsymbol{R_{v,i}}(\mathbf{sin}\,\boldsymbol{\varphi} - \boldsymbol{\psi}\ \mathbf{cos}\,\boldsymbol{\varphi}) \tag{10}$$

where $R_{a,i}$ and $R_{v,i}$ are the screw axial and shear resistance respectively, $\varphi = \varphi_{/\!/}$ and ψ is the coefficient of friction, taken as 0.25 for wood-wood surfaces as per Eurocode 5 [32]. For a shear-compression (SC) STS, the strength is determined similar to a ST STS without the contribution due to friction as:

$$\boldsymbol{F_{A,SC,i}} = \boldsymbol{R^*_{a,i}}\,\mathbf{cos}\,\boldsymbol{\varphi} + \boldsymbol{R^*_{v,i}}\,\mathbf{sin}\,\boldsymbol{\varphi} \tag{11}$$

where $R_{a,i}{}^*$ was calculated similar to $R_{a,i}$ but included the consideration for "edge effect". Jockwer et al. [64] observed that an area from the surface of the timber member was affected by splitting / compression failures such that a zero stress zone exists up until a certain length, x_1. In this way l_{ef} is reduced by x_1, which is defined as the length from the CLT face with zero embedment and withdrawal capacity and determined as:

$$\boldsymbol{x_1} = \boldsymbol{f_{h,\varphi} d_{ef}}/\mathbf{2}\,\mathbf{tan}\,\boldsymbol{\varphi}\,\boldsymbol{f_{rs}} \tag{12}$$

where f_{rs} is the rolling shear strength of the applicable layer. In this instance, f_{rs} is 2.2, 1.1 or 0.9MPa considering the 20, 35, and 45mm layers of the CLT specimens respectively as previously reported by Li et al. [65]. $R_{v,i}{}^*$ is determined as per Jockwer et al. [64] as:

$$\boldsymbol{R^*_{v,i}} = \sqrt{\mathbf{2}\boldsymbol{M_y d_{ef} f_{h,\varphi}} + \left(\boldsymbol{f_{h,\varphi} d_{ef} x_1}\right)^{\mathbf{2}}} - \boldsymbol{f_{h,\varphi} d_{ef} x_1} \tag{13}$$

When ST and SC STS are used together in a X configuration, the strength of a cross-pattern (X) pair of screws is defined similar to Tomasi et al. [34] as:

$$\boldsymbol{F_{A,X,i}} = (\mathbf{R}_{\boldsymbol{a,i}}\,\mathbf{cos}\,\boldsymbol{\varphi} + \boldsymbol{R_{v,i}}\,\mathbf{sin}\,\boldsymbol{\varphi}) + (\boldsymbol{R^*_{a,i}}\,\mathbf{cos}\,\boldsymbol{\varphi} + \boldsymbol{R^*_{v,i}}\,\mathbf{sin}\,\boldsymbol{\varphi}) \tag{14}$$

where $\varphi = \varphi_{\parallel}$ and the contribution from friction from the ST and SC screw are opposite and balance each other. For a X + S configuration, in a similar manner to Tomasi et al. [39], by superposition the strength is determined as:

$$\boldsymbol{F_{A,X+S,i}} = \boldsymbol{n_x F_{A,X,i}} + \boldsymbol{n_s F_{A,S,i}} \tag{15}$$

where $F_{A,X,i}$ and $F_{A,S,i}$ are defined above and n_x and n_s are the number of X pair and S STS respectively.

4.3 Stiffness Model

The analytical stiffness model developed by Tomasi et al. [34] and shown in Eq. **16** with work by Kevarinmaki [38] was adapted herein for orthogonal joint design.

$$\boldsymbol{K_{A,STS} = k_{\perp} sin^2\varphi + k_{\parallel} cos^2\varphi} \tag{16}$$

where $K_{A,STS} = K_{A,S}$, $K_{A,ST}$, *or* $K_{A,SC}$ for a 90°, ST, or SC STS respectively, $\varphi = \varphi_{\parallel}$ as defined before and $k_{\perp}$ is the lateral stiffness component and provided in Eurocode 5 [32] as:

$$\boldsymbol{k_{\perp} = \frac{\rho_m^{1.5} d_{ef}}{23}} \tag{17}$$

where ρ_m is the mean characteristic density and d_{ef} is defined previously. The axial stiffness component, $k_{/\!/}$, is determined following the model proposed by Kevarinmaki [38] which considered the axial stiffness of a screw as a function of the thread stiffness on the middle and side panel side of the screw, similar to a system of two springs in series as:

$$\boldsymbol{k_{\parallel} = \frac{1}{\frac{1}{k_{ax,sp}} + \frac{1}{k_{ax,mp}}}} \tag{18}$$

where $k_{ax,sp}$ and $k_{ax,mp}$ are the axial slip modulus of the side and middle panel of the joint respectively, determined by SPAX ETA [55] as:

$$\boldsymbol{k_{ax} = 25 d l_{ef}} \tag{19}$$

where d and l_{ef} are defined previously. For a 90° STS, $\varphi = 90°$ and the axial component in Eq. **16** reduces to 0. For a SC STS, l_{ef} is reduced by x_1 as defined before. The overall specimen stiffness is determined as per Eq. **20**.

$$\boldsymbol{K_A = n_S K_{A,S} + n_{ST} K_{A,ST} + n_{SC} K_{A,SC}} \tag{20}$$

where n_S, n_{ST}, and n_{SC} are the number of S, ST, and SC STS respectively. $k_{\perp}$ and $k_{/\!/}$ can also be determined from experimental tests as suggested by Blaß et al. [66] instead of empirical component equations. In this way, the overall specimen stiffness could be determined using experimental STS stiffness for $k_{\perp}$ and $k_{/\!/}$ in Eq. **16** and then in Eq. **20** to determine $K_{A/EXP}$.

4.4 Experimental-Analytical Comparison and Discussion

Table 4 summarizes the experimental-analytical comparison results. Using EN 14358 [67] and assuming a log-normal strength distribution, the 5th and 95th percentile strength, $F_{0.05}$ and $F_{0.95}$, were determined from the cyclic test F_y results. The $F_{0.05}$ was compared to the analytical strength F_A, $\gamma_{an} = F_{0.05}/F_A$, and the experimental overstrength, γ_{Rd}, was derived. The average monotonic stiffness, k, was compared to both analytical stiffness

K_A, which was derived from empirical component equations and $K_{A/EXP.}$, which was derived from experimental component stiffness results.

Table 4: Experimental-Analytical Comparisons Summary

Series	$F_{0.05}$	$F_{0.95}$	k	F_A	K_A	γ_{an}	$\gamma_{0.95}$	γ_{Rd}	k/K_A	$k/K_{A/Exp.}$
	kN	kN	kN/mm	kN	kN/mm	-	-	-	-	-
2S	-	-	0.8	6	5	-	-	-	0.2	1.0
8ST	-	-	45	68	38	-	-	-	1.2	2.0
8SC	-	-	33	27	25	-	-	-	1.3	1.7
16X-400	140	222	49	150	104	0.9	1.6	-	0.5	-
16X	108	164	69	81	57	1.3	1.5	2.0	1.2	1.7
16X+16S	154	208	92	132	96	1.2	1.4	1.6	1.0	1.3
12X	139	247	75	140	90	1.0	1.8	1.8	0.8	-
12X+4S	196	284	103	170	104	1.2	1.4	1.7	1.0	-
12X+6S	184	250	102	184	110	1.0	1.4	1.4	0.9	-

The average γ_{an}, which is the ratio between the experimental 5th percentile strength and analytical strength, was 1.1. This shows that the analytical strength model considered in Section 4.2 and used herein was acceptable. The appropriateness of using superposition in Eq. **15** to determine for example $F_{A,16X+16S}$ was calculated considering the 16X and 2S test series average monotonic results. F_{2S} = 7kN was considered at 6mm joint slip because for series 16X and 16X+16S, peak load occurred at approximately 6mm joint slip. For comparison, $F_{max,16X-M} + 8F_{2s} = 209kN$ which is within 15% of $F_{max,16X+16-M}$. Therefore, superposition of mixed angle screws provided reasonable predictions in this instance, as was reported by Tomasi et al. [39]. However, a strength prediction model which can account for the significantly different stiffness of inclined STS and 90° STS is needed to give more accurate prediction results.

The experimental stiffness, k, was compared to analytical stiffness, as per Eq. **20**, considering both empirical component equations to determine K_A and experimental component test results for $k_{\perp}$ and k_{ax} to determine $K_{A/EXP.}$. In general, the analytical stiffness model was inadequate. Although the k/K_A ratio showed that the analytical model appeared to be working well, as noted by Loss et al. [47], the model is very sensitive to the components $k_{\perp}$ and k_{ax}. In determining K_A, $k_{\perp}$ was determined as per Eurocode 5 [32] which had been derived for a traditional wood screw and does not consider the screw type, insertion angle and length of the STS [47]. Reported results herein of k_{2S}/K_A = 0.2, which were similar to past reported lateral stiffness [46,47], indicated that Eq. **17** from Eurocode 5 [32] is not appropriate for STS. As $k_{\perp}$ contributed to both inclined STS and 90° STS this affected the analytical stiffness model. Further, it has been reported that the axial slip modulus, k_{ax}, equations used can provide significant differences up to 500% depending on the screw diameter and insertion length (Ringhofer, 2017). For example, the ∅12x350mm screws could have k_{ax} = 48.9kN/mm or 9.8kN/mm if Eq. **19** or if the equation used in Loss et al. [47] of $k_{ax} = 780d^{0.2}l_{ef}^{0.4}$ was used. As recommended by Blaß et al. [66], as a second comparison, $K_{A/Exp.}$ was determined using experimental STS stiffness for $k_{\perp}$ and k_{ax} and it was compared to experimental results as $k/K_{A/Exp.}$ in Table 4. To determine $K_{A/Exp.}$, $k_{\perp}$ was 1.8kN/mm as reported in Section 3.5 and k_{ax} was 9.5 kN/mm as per Figure 10 to determine $k_{//}$ as per Eq. **18**. Figure 10 shows the reported experimental k_{ax} results of 187 STS withdrawal tests with Ø8mm and Ø12mm STS at various angles to the grain and penetration lengths in comparison to Eq. **19**. The average $k/K_{A/Exp.}$ ratio of 1.7 indicated that the analytical stiffness model of Tomasi et al. [34] underestimated the observed experimental stiffness. That Tomasi et al. [34] observed similar findings with $k/K_A \approx$ up to 2.0 when $k_{//}$ was determined as per Kevarinmaki [38] suggests that further research is required to capture the joint stiffness of STS installed at varying inclinations to grain.

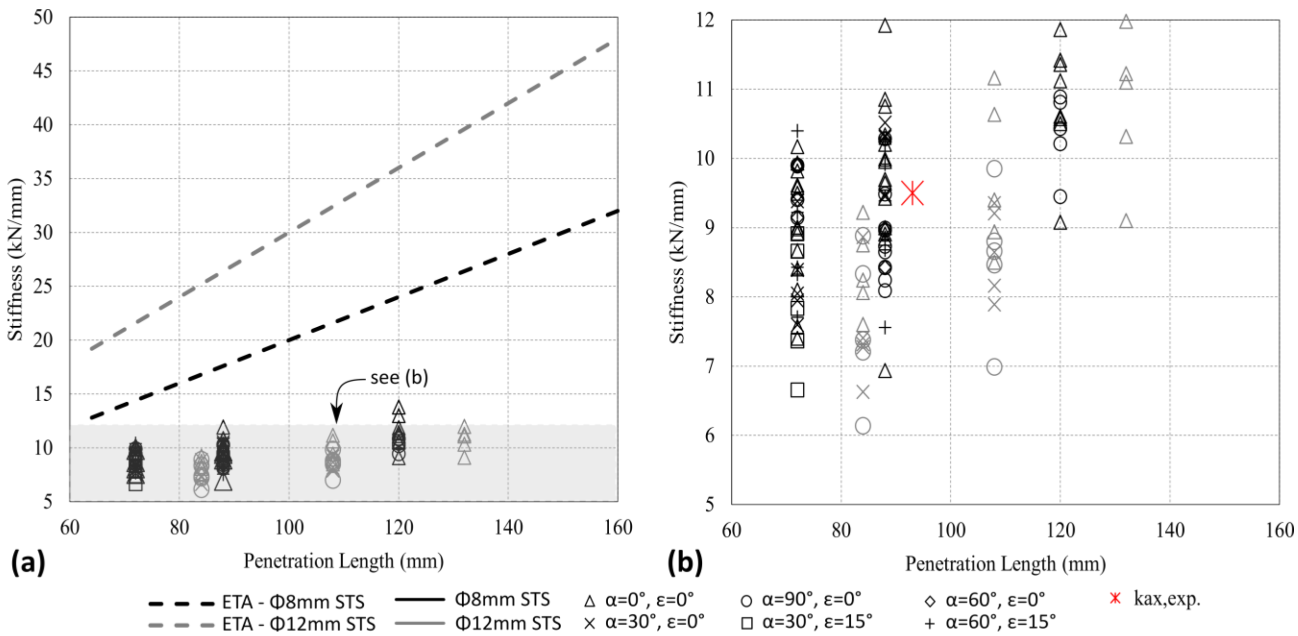

Figure 10: Experimental STS withdrawal stiffness with comparison to empirical equation [57]

4.5 Overstrength Discussion

The overstrength of each test series was calculated as per Eq. **1** assuming $\gamma_m = 1.0$ as per Eurocode 8 [69]. As per Table 4, the average cyclic experimental γ_{Rd} was 1.7 excluding the 16X-400 test series as brittle STS tensile failure occurred. This γ_{Rd} was comparable to past experimental overstrength factors for timber joints [13,28–31]. The slightly higher experimental overstrength reported herein could in part be due to the relatively small sample size as the average $\gamma_{0.95}$ was 1.5. The average γ_{an} was 1.1 which is comparable to γ_{an} = 1.18 [27] and γ_{an} = 1.06 [30]. In a similar manner to Ottenhaus et al. [30], the analytical component overstrength component can be determined as per Eq. **21**.

$$\gamma_{an} = \gamma_{an,cyc}\, \gamma_{fh}\, \gamma_{an,f1} \gamma_{an,My} \tag{21}$$

where $\gamma_{an,cyc.}$ is the ratio of cyclic loading to monotonic loading, $\gamma_{an,fh}$ is overstrength from embedment strength formulation, $\gamma_{an,f1}$ is overstrength from the withdrawal strength parameter, and $\gamma_{an,My}$ is the overstrength from the STS yield moment formulation. The average overstrength observed under cyclic loading, $\gamma_{an,cyc.,}$ was 0.98. For instance, the 16X test series $\gamma_{an,f1}$ was 1.5 when considering the experimental withdrawal strength parameter reported by Brown et al. [57]. A parametric component study of embedment strength and yield moment determination could also define $\gamma_{an,fh}$ and $\gamma_{an,My}$ respectively. It is important to note that the experimentally determined overstrength of this study should only be used for this particular tested joint. A generic analytical component strength overstrength approach such as that developed by Ottenhaus et al. [30] was beyond the scope of this study, though it could provide a strong alternative to costly experimental testing.

5 Conclusions

The paper investigated the performance of orthogonal joints between CLT panels with varying mixed angle STS combination ratios, η, for the purpose of developing enhanced joints between CLT wall panels. A total of 59 specimens consisting of two CLT layups and different STS sizes were tested under monotonic and cyclic loading to determine strength, displacement capacity, ductility, stiffness and overstrength and to compare to analytical predictions. The key findings are summarized as follows:

- Mixed angle STS joints had increased joint displacement capacity, ductility and energy dissipation when compared to inclined only STS joints.
- Based on the test results, a maximum inclined STS to 90° STS η ratio of 2:1 led to more efficient design than the η ratio of 1:1. The 2:1 η ratio ensured high displacement capacity exceeding 20mm, whereas a larger 3:1 or 1:0 η ratio had displacement capacity limited to 13mm or less respectively. Displacement capacity is critical to develop ductility and hysteretic damping under seismic loading. The 2:1 η ratio ensured rope effect by 90° STS at increased joint displacement was significant enough to maintain post-peak strength above 80% F_{max}.
- Strength and stiffness of the mixed angle STS joints was affected by 90° STS. For example, in cyclic series 12X, 12X+4S, and 12X+6S, F_{max} was 195, 247, and 251kN and k was 110, 126 and 151kN/mm respectively. Peak strength in inclined only and mixed angle test series occurred at similar displacements, which can provide one reason for using superposition to estimate the joint strength.
- The average experimental overstrength, γ_{Rd}, was 1.7 excluding 16X-400 where brittle tensile failure occurred. Existing analytical models were found to be adequate in estimating the joint strength using superposition to determine the strength of joints with STS of mixed angles with different stiffness. Further work should verify the suitability of such method.
- Analytical models for estimating joint stiffness were found to be inadequate, especially when considering experimental results for $k_{\perp}$ and k_{ax} from 90° STS and single STS withdrawal tests.
- The preferred failure mode for inclined STS joints is gradual screw withdrawal. It is critical to limit the STS thread embedment such that progressive zipper-like tensile failure is avoided. Except for series 16X-400, screw withdrawal failure was the dominant failure mode which led to moderate to high ductility, μ≥4,

even in the test series with only inclined STS. However, the displacement capacity is limited in joints with inclined only STS and significantly less than joints with η ratio of 0:1, 1:1 and 2:1.

- STS slenderness ratio, λ, was found to influence the joint displacement capacity, ductility, stiffness and energy dissipation capacity. Ø12mm STS with higher λ had increased displacement capacity, ductility, and energy dissipation capacity in terms of equivalent viscous damping than Ø8mm STS. This highlighted the importance of testing larger diameter STS with various λ in larger 7-ply (275mm thick) CLT panels which may be required in taller timber buildings.

While the results presented herein showed mixed angle STS installations could provide enhanced displacement capacity, ductility and energy dissipation, further work is needed to optimize design. Inclined STS without countersinking but with controlled thread embedment length on the STS tip side member could be investigated for similar enhanced performance. A possible group effect for ductile STS joint design should be further investigated. This study provided fundamental information for a better understanding of mixed angle STS joints in orthogonal CLT panels such that in-plane CLT LLRS could transform to core-wall structures with enhanced strength, stiffness and energy dissipation capacity.

Acknowledgements

The authors would like to acknowledge the sponsorship of Speciality Wood Products Partnership, New Zealand Douglas-Fir Association, Australian Research Council Future Timber Hub, SPAX Pacific, and the New Zealand Commonwealth Scholarship and Fellowship Plan. The technical support from Peter Coursey and Gavin Keats and technical comments from Afrin Hossain on experimental set-up are also gratefully acknowledged.

References

[1] Li M, Lam F, Foschi RO. Seismic reliability analysis of diagonal-braced and structural-panel- sheathed wood shear walls. J Struct Eng 2009;135:587–96. https://doi.org/10.1061/(ASCE)ST.1943-541X.0000008.

[2] Li M, Lam F, Foschi RO, Nakajima S, Nakagawa T. Seismic performance of post and beam timber buildings I: Model development and verification. J Wood Sci 2012;58:20–30. https://doi.org/10.1007/s10086-011-1219-5.

[3] Li M, Lam F, Foschi RO, Nakajima S, Nakagawa T. Seismic performance of post-and-beam timber buildings II: Reliability evaluations. J Wood Sci 2012;58:135–43. https://doi.org/10.1007/s10086-011-1232-8.

[4] Green M, Taggart J. Tall wood buildings: design, construction and performance. Boston, United States: Birkhauser; 2017.

[5] Brandner R, Flatscher G, Ringhofer A, Schickhofer G, Thiel A. Cross laminated timber (CLT): overview and development. Eur J Wood Wood Prod 2016;74:331–51.

[6] Pei S, Van De Lindt JW, Popovski M, Berman JW, Dolan JD, Ricles J, et al. Cross-Laminated Timber for Seismic Regions: Progress and Challenges for Research and Implementation. J Struct Eng 2016;142.

[7] Dujic B, Pucelj J, Zarnic R. Testing of racking behavior of massive wooden wall panels. Proc. CIB W18 Meet. Thirty-Seven, Edinburgh, Scotland: 2004.

[8] Amini MO, van de Lindt JW, Rammer D, Pei S, Line P, Popovski M. Systematic experimental investigation to support the development of seismic performance factors for cross laminated timber shear wall systems. Eng Struct 2018;172:392–404. https://doi.org/10.1016/j.engstruct.2018.06.021.

[9] Flatscher G, Bratulic K, Schickhofer G. Experimental tests on cross-laminated timber joints and walls. Proc Inst Civ Eng - Struct Build 2015;168:868–77. https://doi.org/10.1680/stbu.13.00085.

[10] Gavric I, Ceccotti A, Fragiacomo M, Popovski M. Behaviour of Cross-Laminated Timber Panels under Cyclic Loads. Mater Joints Timber Struct Recent Dev Technol 2014:689–702.

[11] Gavric I, Fragiacomo M, Ceccotti A. Cyclic Behavior of CLT Wall Systems: Experimental Tests and Analytical Prediction Models. J Struct Eng 2015;141:4015034. https://doi.org/doi:10.1061/(ASCE)ST.1943-541X.0001246.

[12] Popovski M, Schneider J, Schweinsteiger M. Lateral load resistance of cross-laminated wood panels. WCTE 2010, vol. 4, Riva Del Garda, Italy: 2010, p. 3394–403.

[13] Dong W, Li M, Ottenhaus LM, Lim H. Ductility and overstrength of nailed CLT hold-down connections. Eng Struct 2020;215:110667. https://doi.org/10.1016/j.engstruct.2020.110667.

[14] Liu J, Lam F, Foschi RO, Li M. Modeling the Coupling Effect of CLT Connections under Biaxial Loading. J Struct Eng 2020;146:1–13. https://doi.org/10.1061/(ASCE)ST.1943-541X.0002589.

[15] Tannert T, Follesa M, Fragiacomo M, González P, Isoda H, Moroder D, et al. Seismic design of cross-laminated timber buildings. Wood Fiber Sci 2018;50:3–26.

[16] Wood Solutions. 2019 changes to the National Construction Code (NCC) 2019. https://www.woodsolutions.com.au/blog/2019-changes-national-construction-code-ncc (accessed May 8, 2020).

[17] NRC. Proposed Changes to 2020 NBCC. 2018.

[18] Breneman S, Richardson D. Tall Wood Buildings and the 2021 IBC: Up to 18 Stories of Mass Timber. WoodWorks 2019.

[19] New Zealand Government. Climate Change Response (Zero Carbon) Amendment Act 2019. Wellington, New Zealand: 2019.

[20] Rotorua Lakes Council. Wood First Policy. Rotorua Lakes Council: 2015.

[21] Gisborne District Council. Wood first policy for Gisborne District Council. Gisborne, New Zealand: 2018.

[22] Buchanan A. The challenges for designers of tall timber buildings. WCTE 2016 - World Conf. Timber Eng., Vienna, Austria: 2016.

[23] Ottenhaus L, Li M, Smith T. Analytical Derivation and Experimental Verification of Overstrength Factors of Dowel-type Timber Connections for Capacity Design Analytical Derivation and Experimental Verification of. J Earthq Eng 2020;00:1–15. https://doi.org/10.1080/13632469.2020.1781711.

[24] Smith T, Moroder D, Sarti F, Pampanin S, Buchanan A. The Reality of Seismic Engineering in a Modern Timber World. Proc. INTER Meet. Forty-Eight, vol. 48-102–03, Sibenik, Croatia: 2015.

[25] McDonnell E, Jones B. Performance-Based Engineering Provides Path to More Compelling Mass Timber Projects. Technol Archit Des 2020;4:9–13. https://doi.org/10.1080/24751448.2020.1705709.

[26] Casagrande D, Doudak G, Polastri A. A proposal for the capacity-design at wall- and building-level in light-frame and cross-laminated timber buildings. Bull Earthq Eng 2019;17:3139–67. https://doi.org/10.1007/s10518-019-00578-4.

[27] Jorissen A, Fragiacomo M. General notes on ductility in timber structures. Eng Struct 2011;33:2987–97. https://doi.org/10.1016/j.engstruct.2011.07.024.

[28] Bruhl F, Schanzlin J, Kuhlmann U. Ductility in Timber Structures: Investigations on Over-Strength Factors. Dordrecht, Netherlands: Springer; 2014. https://doi.org/10.1007/978-94-007-7811-5.

[29] Gavric I, Fragiacomo M, Ceccotti A. Cyclic behavior of typical screwed connections for cross-laminated (CLT) structures. Eur J Wood Wood Prod 2015;73:179–91.

[30] Ottenhaus LM, Li M, Smith T, Quenneville P. Overstrength of dowelled CLT connections under monotonic and cyclic loading. Bull Earthq Eng 2018:1–21. https://doi.org/10.1007/s10518-017-0221-8.

[31] Ottenhaus L-M, Li M, Smith T. Structural performance of large-scale dowelled CLT connections under monotonic and cyclic loading. Eng Struct 2018;176:41–8. https://doi.org/10.1016/j.engstruct.2018.09.002.

[32] CEN. Eurocode 5: Design of timber structures-Part 1-1: General-Common rules and rules for buildings. EN1995-1-12004-11 + AC2006-06 + A12008-06 + A22014-05 Eurocode 5 2014.

[33] Dorn M, de Borst K, Eberhardsteiner J. Experiments on dowel-type timber connections. Eng Struct 2013;47:67–80. https://doi.org/10.1016/j.engstruct.2012.09.010.

[34] Tomasi R, Crosatti A, Piazza M. Theoretical and experimental analysis of timber-to-timber joints connected with inclined screws. Constr Build Mater 2010;24:1560–71. https://doi.org/https://doi.org/10.1016/j.conbuildmat.2010.03.007.

[35] Hossain A, Popovski M, Tannert T. Group Effects for Shear Connections with Self-Tapping Screws in CLT. J Struct Eng (United States) 2019;145:1–9. https://doi.org/10.1061/(ASCE)ST.1943-541X.0002357.

[36] Dietsch P, Brandner R. Self-tapping screws and threaded rods as reinforcement for structural timber elements-A state-of-the-art report. Constr Build Mater 2015;97:78–89. https://doi.org/10.1016/j.conbuildmat.2015.04.028.

[37] Bejtka I, Blaß HJ. Joints with inclined screws. CIB-W18 Timber Struct. Meet. 35, vol. 35-7–4, Kyoto, Japan: 2002, p. 141.

[38] Kevarinmaki A. Joints with Inclined Screws. CIB-W18 Timber Struct. Meet. 35, vol. 35-7–3, Kyoto, Japan: 2002.

[39] Tomasi R, Piazza M, Angeli A, Mores M. A new ductile approach design of joints assembled with screw connectors. WCTE 2006, Portland, USA: 2006.

[40] Mohammad M, Blaß HJ, Salenikovich A, Ringhofer A, Line P, Rammer D, et al. Design Approaches for CLT Connections. Wood Fiber Sci 2018;50:27–47.

[41] Ringhofer A, Brandner R, Blaß HJ. Cross laminated timber (CLT): Design approaches for dowel-type fasteners and connections. Eng Struct 2018. https://doi.org/10.1016/j.engstruct.2018.05.032.

[42] Uibel T, Blaß HJ. Load carrying capacity of joints with dowel type fasteners in solid wood panels. Proc. CIB W18 Meet. Thirty-Nine, Florence, Italy: 2006, p. 191–202.

[43] Uibel T, Blaß HJ. Edge joints with dowel type fasteners in cross laminated timber. Proc. CIB W18 Meet. Forty, Bled, Slovenia: 2007.

[44] Hossain A, Danzig I, Tannert T. Cross-laminated timber shear connections with double-angled self-tapping screw assemblies. J Struct Eng 2016;142.

[45] Hossain A, Popovski M, Tannert T. Cross-laminated timber connections assembled with a combination of screws in withdrawal and screws in shear. Eng Struct 2018;168:1–11. https://doi.org/10.1016/j.engstruct.2018.04.052.

[46] Sullivan K, Miller TH, Gupta R. Behavior of cross-laminated timber diaphragm connections with self-tapping screws. Eng Struct 2018;168:505–24.

[47] Loss C, Hossain A, Tannert T. Simple cross-laminated timber shear connections with spatially arranged screws. Eng Struct 2018;173:340–56. https://doi.org/10.1016/j.engstruct.2018.07.004.

[48] Connolly T, Loss C, Iqbal A, Tannert T. Feasibility study of mass-timber cores for the UBC tall wood building. Buildings 2018;8. https://doi.org/10.3390/buildings8080098.

[49] Polastri A, Izzi M, Pozza L, Loss C, Smith I. Seismic analysis of multi-storey timber buildings braced with a CLT core and perimeter shear-walls. Bull Earthq Eng 2019;17:1009–28. https://doi.org/10.1007/s10518-018-0467-9.

[50] Moroder D, Smith T, Dunbar A, Pampanin S, Buchanan A. Seismic testing of post-tensioned Pres-Lam core walls using cross laminated timber. Eng Struct 2018;167:639–54. https://doi.org/10.1016/j.engstruct.2018.02.075.

[51] Below K, Sarti F. Cathedral hill 2: Challenges in the design of a tall all-timber building. WCTE 2016 - World Conf. Timber Eng., Vienna, Austria: 2016.

[52] Brown J, Li M, Palermo A, Pampanin S, Sarti F. Seismic testing of post-tensioned flanged CLT core-walls. Forthcoming. J Struct Eng n.d. https://doi.org/10.1061/(ASCE)ST.1943-541X.0002926.

[53] Brown J, Li M, Nokes R, Palermo A, Pampanin S, Sarti F. Investigating the compressive toe of pos-tensioned CLT core-walls use Particle Tracking Technology. 17th World Conf. Earthq. Eng. 17WCEE, Sendai, Japan: 2020.

[54] Standards New Zealand. NZS 3603: Timber structures standard. Private Bag 2439, Wellington, New Zealand: Standards New Zealand; 1993.

[55] ETA. ETA-12/0114: SPAX self-tapping screws - screws for use in timber constructions. Nordhavn, Danmark: ETA-Danmark A/S; 2017.

[56] Hossain A, Popovski M, Tannert T. Group effect for self-tapping-screw in CLT, subjected to shear and axial loads. WCTE2018 2018.

[57] Brown J, Li M, Karalus B, Stanton S. Withdrawal Behaviour of Self-tapping Screws in New Zealand Cross-Laminated Timber. New Zeal Timber Des J 2020;28.

[58] Ringhofer A, Brandner R, Schickhofer G. Withdrawal resistance of self-tapping screws in unidirectional and orthogonal layered timber products. Mater Struct 2015;48:1435–47.

https://doi.org/10.1617/s11527-013-0244-9.

[59] Standards New Zealand. NZS 3404: Steel Structures Standard. Private Bag 2439, Wellington, New Zealand: Standards New Zealand; 1992.

[60] CEN. EN 26891 - Joints made with mechanical fasteners. General principles for the determination of strength and deformation characteristics. Brussels, Belgium: European Committee for Standardization (CEN); 1991.

[61] CEN. EN12512: Timber structures: test methods : cyclic testing of joints made with mechanical fasteners : [including amendment A1:2005]. Brussels: European Committee for Standardization; 2005.

[62] Smith I, Asiz A, Snow M, Chui YH. Possible Canadian / ISO Approach to Deriving Design Values From Test Data. Proc. CIB W18 Meet. Thirty-Nine, Florence, Italy: 2006.

[63] Flatscher G. Evaluation and approximation of timber connection properties for displacement-based analysis of CLT wall systems. 2017.

[64] Jockwer R, Steiger R, Frangi A. Design model for inclined screws under varying load to grain angles. Int. Netw. Timber Eng. Res. - Meet. 47, Bath, United Kingdom: 2014, p. 141–54.

[65] Li M, Dong W, Lim H. Influence of Lamination Aspect Ratios and Test Methods on Rolling Shear Strength Evaluation of Cross-Laminated Timber. J Mater Civ Eng 2019;31:1–11. https://doi.org/10.1061/(ASCE)MT.1943-5533.0002977.

[66] Blaß HJ, Bejtka I, Uibel T. Tragfähigkeit von Verbindungen mit selbstbohrenden Holzschrauben mit Vollgewinde(In German). number 4. Karlsruher Berichte zum Ingenieurholzbau Universitätsverlag Karlsruhe; 2006.

[67] CEN. EN 14358:2016 - Timber structures - Calculation and verification of characteristic values. Brussels, Belgium: European Committee for Standardization (CEN); 2016.

[68] Ringhofer A. Axially Loaded Self-Tapping Screws in Solid Timber and Laminated Timber Products. Timber Engineering & Technology, TET 5, Verlag der Technischen Universität Graz; 2017. https://doi.org/10.3217/978-3-85125-555-3.

[69] CEN. Eurocode 8: Design of structures for earthquake resistance. Brussels, Belgium: European Committee for Standardization (CEN); 2005.